Ligand-Controlled Dissociation of *Chromatium vinosum* Cytochrome *c'* †

Michael L. Doyle and Stanley J. Gill*

Department of Chemistry and Biochemistry, University of Colorado, Boulder, Colorado 80309

Michael A. Cusanovich

Department of Biochemistry, University of Arizona, Tuscon, Arizona 85721

Received October 7, 1985; Revised Manuscript Received December 6, 1985

ABSTRACT: Carbon monoxide binding to *Chromatium vinosum* ferrocytochrome *c'* has been studied by high-precision equilibrium methods. In contrast to the CO binding properties of *Rhodospirillum molischianum* cytochrome *c'* [Doyle, M. L., Weber, P. C., & Gill, S. J. (1985) *Biochemistry 24*, 1987–1991], CO binding to *C. vinosum* cytochrome *c'* is found to be unusual in the following ways. (1) The binding curve is found to be cooperative with typical Hill coefficients equal to 1.25. (2) The shape of the binding curve is asymmetrical. (3) The heat of CO ligation is measured by two independent methods, both of which yield large endothermic values of approximately 10 kcal [mol of CO(aq)]$^{-1}$. (4) The overall affinity for CO increases as the concentration of cytochrome *c'* decreases. These observations suggest the CO binding properties of *C. vinosum* cytochrome *c'* are complicated by CO-linked association–dissociation processes. Further investigation by gel filtration chromatography shows that at micromolar concentrations the dimeric state is tightly associated in both the reduced and oxidized forms of the cytochrome but addition of saturating concentrations of CO causes the reduced ligated dimer to dissociate largely into monomers. A model is presented that quantitatively fits the data, involving a ligand-linked dimer–monomer dissociation reaction. In this model, CO binds to the dimer form noncooperatively with an intrinsic affinity constant equal to 5600 ± 1200 M^{-1} at 25 °C. The unligated dimer form is tightly associated, but addition of CO causes dissociation of the dimer into the monomer with a monomer–dimer association constant equal to 450 ± 200 M^{-1}. A normal enthalpy change of −9 ± 5 kcal/mol of CO(aq) is found for the dimer form and an enthalpy change of −38 ± 10 kcal/mol of dimer for association of the ligated monomer to fully ligated dimer. An unexpected observation is that the total enthalpy change for CO ligation of the reduced dimer form to yield mainly ligated monomer, measured directly by calorimetry, is equal to 20 ± 5 kcal/mol of dimer. From the observed standard free energy change of dissociation of the ligated species (3.6 kcal/mol of dimer) one finds a large entropy change of 130 cal/(deg·mol of dimer). Exposure of hydrophobic groups to solvent upon dissociation of the dimer into monomers would be expected to give an entropy change of opposite sign. Thus, one concludes that significant structural changes occur within the subunits in going from ligated dimeric to monomeric forms.

The cytochromes *c'* are a group of heme proteins isolated from a wide variety of photosynthetic and denitrifying bacteria (Bartsch, 1978). The majority of studies on the cytochromes *c'* have been in the area of their unique physical properties, with an excellent summary of this work provided by Meyer and Kamen (1982). The ligand binding reactions for the cytochromes *c'* are unique in that although they are high-spin heme proteins like hemoglobin and myoglobin, they do not bind ionic ligands in the ferric form and their reactions with oxygen and nitric oxide are irreversible (Bartsch, 1978; Taniguchi & Kamen, 1963). Reversible binding studies have recently been reported on ethyl isocyanide binding by some cytochromes *c'* (Kassner et al., 1983; Rubinow & Kassner, 1984), and reversible carbon monoxide binding is ubiquitous among the cytochromes *c'*. Yet, among the cytochromes *c'* there are large differences in CO binding, both in terms of kinetics and in terms of overall affinity (Cusanovich & Gibson, 1973).

The present investigation continues our study of possible allosteric interactions for CO binding in cytochrome *c'* molecules. This work extends the initial high-precision study on the dimer molecule *Rhodospirillum molischianum* cytochrome *c'* (Doyle et al., 1985), for which X-ray structural information was available, to the cytochrome *c'* from the purple photosynthetic bacterium *Chromatium vinosum*. This cytochrome *c'* is also a dimeric heme protein (Cusanovich, 1971) consisting of two identical subunits (Kennel et al., 1972). The dimeric form is tightly associated in both the oxidized and reduced forms and unaffected by 6 M guanidine hydrochloride (Gdn-HCl) (Cusanovich, 1971). The kinetics of carbon monoxide binding by *C. vinosum* cytochrome *c'* are complex, involving at least three separate second-order processes, and an unusual stoichiometry for the overall reaction has been suggested to be two CO molecules per subunit (Cusanovich & Gibson, 1973). This is in contrast to *R. molischianum* cytochrome *c'* where CO binding is described by a simple one-step kinetic process (M. A. Cusanovich, unpublished results) and the stoichiometry of ligation has been found equal to one CO molecule per heme (Doyle & Gill, 1985). High-precision binding curve measurements for CO binding to *C. vinosum* ferrocytochrome *c'* have been performed to examine possible cooperative effects and to determine the thermodynamic parameters of the binding reactions for this system in detail. The enthalpy change of the CO binding reaction has also been characterized by titration calorimetry. In the course of these investigations it became apparent that the normal dimeric state of the unligated molecule was converted to a monomeric state in the presence of carbon monoxide. Gel

† This work was supported by National Institutes of Health Grants HL 22325 (S.J.G.) and GM 21277 (M.A.C.).

0006-2960/86/0425-2509$01.50/0

filtration studies were carried out to test for CO-linked changes in molecular weight.

A ligand-regulated dimer–monomer process has been found to accurately describe the observed ligand binding properties for the *C. vinosum* system. Such ligand-linked dissociation processes have been demonstrated in the more complicated oxygen-linked tetramer–dimer process found in hemoglobin (Ackers & Halvorson, 1974). The dimeric form of the cytochromes *c'* greatly simplifies the thermodynamic characterization of the system and provides perhaps the simplest situation that one can envision for the investigation of the energetics of site–site interaction processes.

Materials and Methods

Chromatium vinosum cytochrome *c'* was prepared according to the method of Bartsch (1971) and then dialyzed against 100 mM phosphate buffer. The pH was adjusted by addition of either acetic acid or potassium hydroxide. The enzymatic reducing system of Hayashi et al. (1973) was used to ensure complete reduction of the cytochrome sample throughout the experiment. All components of the system were products of Sigma Chemical Co. This method of reduction is milder and more suitable for our thin-layer technique than the typically used reductant dithionite. Characteristic CO-bound spectra were recorded prior to each experiment in the Soret region with a Cary 219 spectrophotometer.

A thin-layer optical cell (Dolman & Gill, 1978), holding the cytochrome *c'* solution between a glass window and a transparent gas-permeable membrane, was used to study the CO binding reaction. The reaction was monitored at a wavelength of 418 nm with the Cary 219 spectrophotometer. The thickness of the protein solution was 0.002 in., and the concentrations of the protein ranged from 20 to 250 μM heme. The thin-layer cell measures binding curve data to a high degree of precision largely due to the ability of accurately diluting the partial pressure of gaseous ligand. At the beginning of each experiment, the cell was filled with CO to atmospheric pressure. The partial pressure of CO was then accurately diluted through a series of "steps" with nitrogen, by means of a precision dilution valve connected to the cell. The dilution valve dilutes the partial pressure of CO by a factor of 0.706 at each stepwise dilution. Each step required about 5 min for the solution to reach equilibrium.

The optical density change resulting from a given stepwise dilution in CO partial pressure may be computed from the difference in the fraction of sites bound with CO for the initial and final values of partial pressure for a given step times the parameter representing the total optical density change for complete CO ligation of the reduced protein. The measured optical density change, $\Delta OD(i)$, for the ith dilution step, where the CO partial pressure changes from $P_{CO}(i-1)$ to $P_{CO}(i)$ is then described in general terms by the expression

$$\Delta OD(i) = \Delta OD(t)[\theta(i-1) - \theta(i)] \quad (1)$$

Here $\theta(i)$ and $\theta(i-1)$ are the final and initial fractional saturation values for the ith dilution step and $\Delta OD(t)$ is the total optical density change for complete ligation of the reduced protein.

The experimentally determined changes in optical density data at each ith dilution step were represented as a Hill plot (Hill, 1910) by calculating the fraction of sites occupied with CO, $\theta(i)$:

$$\theta(i) = \theta(0) - \frac{\sum_{j=0}^{i} \Delta OD(j)}{\Delta OD(t)} \quad (2)$$

The fraction of sites occupied at the end of the ith step is given as $\theta(i)$. The numerator in eq 2 represents the summation of optical density changes over j for each ith stepwise dilution of the partial pressure of CO. The fraction of sites occupied at the beginning of the experiment, $\theta(0)$, where the pressure of CO is equal to atmospheric pressure minus the vapor pressure of water in the cell (24 torr at 25 °C), was calculated by using the best-fit parameters given in Table I and is typically about 0.98. The fraction of sites occupied at the ith step, $\theta(i)$, was then used to produce the Hill plot in Figure 8.

The overall enthalpy change for CO ligation to the reduced dimer state was measured directly by using a titration microcalorimeter. The details of the calorimeter have been described elsewhere (McKinnon et al., 1984). The materials were prepared for calorimetry by the following procedures. Reduced cytochrome *c'* was prepared by adding the enzymic reducing system of Hayashi et al. (1973) and then flushing the mixture with nitrogen gas to remove oxygen. After 1 h of flushing, the sample was fully reduced as monitored spectrophotometrically in the Soret region. The concentration of cytochrome *c'* was determined prior to reduction on an aliquot of the sample using an extinction coefficient of 85 mM^{-1} cm^{-1} (Bartsch, 1971). A CO-saturated buffer was made from the buffer used in the dialysis of the cytochrome sample by equilibration with atmospheric pressure of CO. The concentration of CO in the buffer was calculated from solubility data (Wilhelm et al., 1977). Aliquots of the reduced cytochrome sample were then injected into the CO-saturated buffer to yield the overall heat of CO ligation. Under the experimental solution conditions the cytochrome becomes 98% saturated with CO.

Gel filtration experiments were carried out with a Beckman Model 332 HPLC using a Bio-Sil TSK-125 column (Bio-Rad). The buffer was 50 mM potassium phosphate, pH 7.0, and the standards used were bovine serum albumin (BSA), *Rhodospirillum rubrum* cytochrome *c'*, *Chromatium vinosum* high-potential iron–sulfur protein, and horse heart cytochrome *c*. Ferrocytochrome *c'* and carboxycytochrome *c'* were run with the buffer given above made 1 mM in sodium dithionite and 1 mM sodium dithionite saturated with CO, respectively, after degassing the buffer with water-saturated argon.

Results

Typical binding data taken with the thin-layer cell are shown in Figure 1 as changes in optical density as a function of stepwise dilution of the partial pressure of CO. The theoretical line shown in this figure is based on a nondissociating two-site Adair model (Adair, 1925). This line has a small but systematic deviation from the observed data points. The important observation is that the binding curve for *C. vinosum* cytochrome *c'* displays positive cooperativity. The optical density data in Figure 1 are converted directly to the Hill plot form using eq 2 and are shown in Figure 8 where the maximum slope is equal to 1.21.

The effect of protein concentration on CO binding is revealed in Figure 2 by the observed shifts in the optical density change functions for three different concentrations of protein. The theoretical curves were generated by using a CO-linked monomer–dimer model to be discussed later. The median CO partial pressure values, p_m, where the area above the binding curve is equal to the area below (Wyman, 1965), is shown in Figure 3 for binding curve studies conducted at various temperatures (20, 25, 30, and 35 °C) and three different protein concentrations (20, 70, and 250 μM heme) at each temperature. Again the solid lines are based on the monomer–dimer model to be discussed later. The most striking feature about

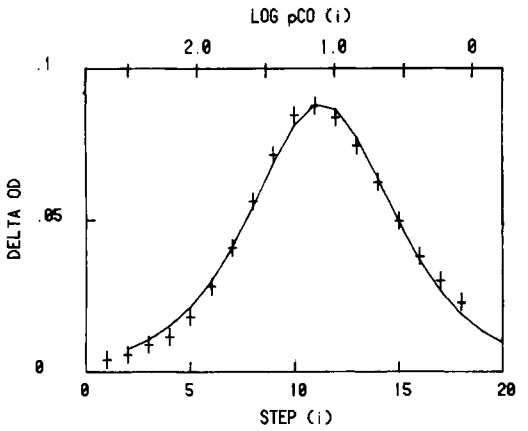

FIGURE 1: Optical density changes for carbon monoxide binding to *C. vinosum* ferrocytochrome *c′*. Experimental conditions were 100 mM potassium phosphate, pH 7.2, 25 °C, and starting partial pressure of CO equal to 608 torr, and the concentration of macromolecule was 20 μM in heme. Changes in optical density are plotted vs. step *i* [where the partial pressure of CO is changed from $p_{CO}(i-1)$ to $p_{CO}(i)$, by a factor of 0.706] along the lower abscissa. The corresponding logarithm of the partial pressure of CO at the end of a given step, $p_{CO}(i)$, is plotted along the upper abscissa. The solid curve is the theoretical two-site binding function, generated with the fitted overall Adair equilibrium constants, $\beta_1 = 9.3 \times 10^{-2}$ torr^{-1} and $\beta_2 = 5.4 \times 10^{-3}$ torr^{-2}. The data are represented as crosses with vertical lines equal to twice the standard error of the least-squares fit to the two-site reaction equation, equal to 2.5×10^{-3} OD unit.

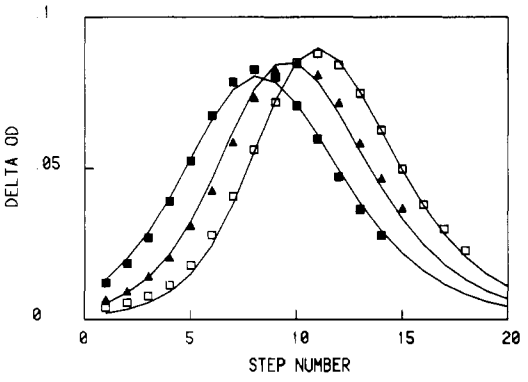

FIGURE 2: Heme concentration dependence for CO binding to *C. vinosum* ferrocytochrome *c′* measured by optical density changes. Solution conditions were pH 7.2, 100 mM potassium phosphate, and 25 °C. The concentrations of protein were (solid squares) 250, (solid triangles) 70, and (open squares) 20 μM heme. The optical density changes for the 20 μM data set are experimental values, and the optical density changes for the other two data sets are scaled to the same total optical density change as the 20 μM set (0.818 OD). All three sets of binding data were fitted simultaneously to eq 1 by using the expression for θ given in eq 5 and 6. The theoretical curve was generated with the fitted intrinsic equilibrium constants, $\kappa_D = 7.1 \times 10^{-3}$ torr^{-1} and $L_2 = 450$ M^{-1}. The standard error of a point for the fit is 1.4×10^{-3} ΔOD unit.

the temperature dependence is that the heat of CO ligation is endothermic. The sign of the enthalpy change is in direct contrast to typical exothermic heats of CO ligation such as for *R. molischianum* cytochrome *c′*, −11 kcal/mol of CO(aq) (Doyle et al., 1985), and the globins, −16 kcal/mol of CO(aq) (Antonini & Brunori, 1971).

Titration calorimetry was used as an independent approach to verify the endothermic heat of reaction implied by the van't Hoff studies. The data shown in Figure 4 represent the total heat observed when aliquots of ferrocytochrome *c′* are injected into a buffer equilibrated with atmospheric pressure of CO. Under these conditions the heme binding sites are 98% bound with CO and the observed total heat of CO ligation is measured directly as 10 ± 2 kcal/mol of heme. The endothermic

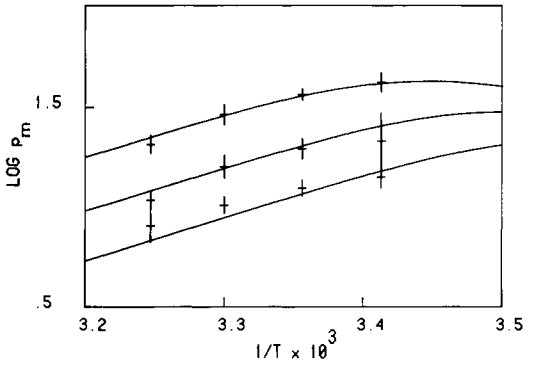

FIGURE 3: Logarithm of the median pressure, p_m, plotted as a function of the inverse of temperature for three protein concentrations. The upper data represent a protein concentration of 250 μM heme, the middle data are for 70 μM heme, and the lower data are for 20 μM heme. Experimental conditions were pH 7.2, 100 mM potassium phosphate buffer, and 25 °C. The p_m values are experimental values determined by integration of the binding curve. Data are represented as crosses with vertical lengths equal to twice the standard error in determining the p_m values. The solid lines are theoretical curves generated from the CO-linked monomer–dimer equilibrium by using the equilibrium constants in Table I.

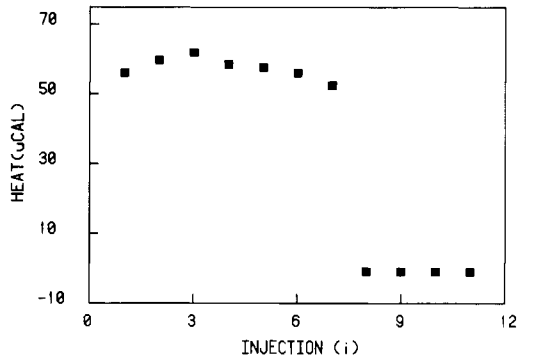

FIGURE 4: Direct measurement of the heat of CO ligation to *C. vinosum* ferrocytochrome *c′* by calorimetry. Solution conditions are 100 mM potassium phosphate, 25 °C, and pH 7.3. The first seven data points represent the heat absorbed when 15-μL aliquots of the cytochrome sample at a concentration of 460 μM heme are injected and stirred into buffer containing CO at an initial concentration of 77 μM. The last four data points are blank values, representing heats of stirring only.

heat of CO ligation to *C. vinosum* cytochrome *c′* indicates that the reaction is more complex than a typical CO binding reaction and is suggestive of ligand-linked changes in quaternary structure.

Independent verification of CO-linked changes in molecular weight for *C. vinosum* cytochrome *c′* was sought by gel chromatography experiments under various conditions of ligation. Figure 5 shows the elution profile of the ferri and ferro (Figure 5a), fully saturated carbonmonoxy (Figure 5b), and partially saturated carbonmonoxy (Figure 5c) forms of *C. vinosum* cytochrome *c′*. The ferri and ferro forms had identical elution profiles and yield an apparent molecular weight of 35 000. This experiment was conducted in the absence of CO on protein concentrations in the range 50–0.1 μM heme with no indication of the dimer dissociating into monomer. An identical apparent molecular weight is obtained in gel filtration experiments in the same buffer using G-100 with ferricytochrome *c′* from *C. vinosum*. As can be seen in Figure 5a a small amount of tetramer is present. On addition of saturating amounts of CO, Figure 5b shows that the tetramer form is diminished and the bulk of the material is converted to a species with an apparent molecular weight of 17 000. Figure 5c shows that partial saturation of the protein with CO con-

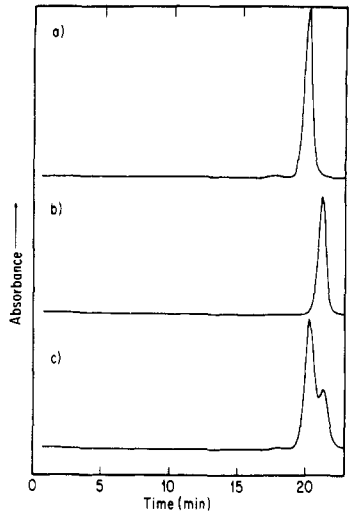

FIGURE 5: Gel filtration of *Chromatium vinosum* cytochrome *c'*. A Bio-Sil T5-125 column (300 mm × 7.5 mm) was used. The buffer was 150 mM potassium phosphate, pH 7.0, and the flow rate was 0.5 mL/min. The concentration of protein for the data shown was about 5 μM. Similar results were observed over the range 50–0.1 μM heme. (a) Oxidized and reduced cytochrome *c'*. For the reduced protein the buffer was made 1 mM in sodium dithionite. (b) Carboxy cytochrome *c'*. (c) Partially carbon monoxide saturated sample. A sample of reduced cytochrome *c'* saturated with CO was injected which was first equilibrated with buffer plus 1 mM sodium dithionite (no CO).

verts a smaller fraction of the protein from dimer to monomer. Cytochrome *c'* from *Rhodospirillum molischianum*, which has no cooperativity in its CO binding curve (Doyle et al., 1985), shows no change in its apparent molecular weight in control experiments. These latter experiments were carried out under identical conditions as those used for *C. vinosum* cytochrome *c'* and gave an apparent molecular weight of 28 000 for ferricytochrome *c'* and 27 000 for the carboxy form (data not shown). Thus, the CO-linked association–dissociation process is not a general property of all cytochromes *c'*.

DISCUSSION

Binding Model. Our findings show that the CO binding reaction to *Chromatium vinosum* cytochrome *c'* is unusual by several criteria. (1) The binding process is cooperative. (2) The heat of reaction for CO ligation is endothermic. (3) The binding curve depends on the concentration of cytochrome. (4) Detailed analysis of the binding curve reveals that it is asymmetrical. Since these criteria are disallowed by a two-site nondissociating model, a more complex mechanism must be considered.

These unusual CO binding properties of *C. vinosum* cytochrome *c'* imply a linkage between CO ligation and an equilibrium between different aggregate forms of the macromolecule. Furthermore, the gel filtration experiments confirm this suggestion and identify the association–dissociation equilibrium involved as one between dimer and monomer forms. A general Adair binding model has been previously developed for the oxygen-linked equilibrium between dimer and tetramer forms of hemoglobin (Ackers & Halvorson, 1974). This model, in a simplified form, provides the basis for a similar interpretation of the CO binding curve properties of *C. vinosum* ferrocytochrome *c'*.

We shall assume the CO-linked equilibrium is between monomer and dimer forms of the macromolecule. Previous work on the CO binding reaction to the nondissociating dimer *R. molischianum* cytochrome *c'* demonstrated that its CO binding curve is noncooperative (Doyle et al., 1985). Thus, we assume that the dimer form of *C. vinosum* cytochrome *c'* also binds CO without cooperativity. Figure 5a shows the presence of a small amount of tetramer. Since this amount is very small, its contribution to the CO binding curve is excluded from the present analysis.

The scheme shown in eq 3 describes the species of ligated and unligated forms of the reduced cytochrome *c'* given by the ligand-linked dissociation model. The various ligated

$$\begin{array}{ccc} [M] + [M] & \xrightarrow{L_0} & [D] \\ \downarrow\kappa_M & & \downarrow\kappa_D \\ [MX] + [M] & \xrightarrow{L_1} & [DX] \\ \downarrow\kappa_M & & \downarrow\kappa_D \\ [MX] + [MX] & \xrightarrow{L_2} & [DX_2] \end{array} \qquad (3)$$

species of the monomer are shown in the left-hand column and those of the dimer in the right-hand column. The association constants of the unligated, singly ligated, and doubly ligated monomer–dimer equilibria are given by L_0, L_1, and L_2, respectively. The intrinsic affinity constants for binding CO (designated as X) to the monomer and dimer forms are shown as κ_M and κ_D, respectively.

The binding curve for this multiple-equilibrium system can be conveniently analyzed in terms of its binding partition function. This binding partition function is equal to the summation of the concentrations of all ligated and unligated macromolecular species. Initially we fit our binding curve data with the complete model shown in eq 3. However, we later learned from the gel chromatography experiments (Figure 5) that the unligated monomer species is essentially nonexistent under the experimental solution conditions studied. The binding curve data were taken from protein concentrations of 20, 70, and 250 μM heme, yet the chromatography studies did not reveal any unligated monomer even at much lower concentrations. Thus, we cannot justify including an extra parameter representing the unligated monomer species into the binding partition function used to analyze the present data. The appropriate partition function, excluding the unligated monomer species, can be written in reference to the concentration of the unligated dimer form, [D], according to the mass law relations in eq 3. This binding partition function, Q, is

$$Q = [D](1 + \kappa_D a_x)^2 + \frac{\sqrt{[D]}\kappa_D a_x}{\sqrt{L_2}} \qquad (4)$$

where a_x is the CO activity in torr.

Binding curves are conveniently represented as the fractional saturation of binding sites on the macromolecule, θ, vs. the activity of ligand, a_x. The fraction of sites bound is related to the binding partition function by the partial derivative of Q with respect to the logarithm of the free ligand activity (Wyman, 1965). This derivative gives the concentration of ligand bound in the system and, if divided by the total concentration of sites, m_0, gives the fraction of sites bound:

$$\theta = \frac{\dfrac{\partial Q}{\partial \ln a_x}}{m_0} = \frac{2\kappa_D a_x[D] + 2\kappa_D^2 a_x^2[D] + \dfrac{\sqrt{[D]}\kappa_D a_x}{\sqrt{L_2}}}{m_0} \qquad (5)$$

The concentration of unligated dimer, [D], is an unknown quantity in the numerator of eq 5 and must be calculated from the mass balance of the system. Since the total concentration

Table I: Thermodynamic Parameters for CO Binding to *C. vinosum* Cytochrome *c′*

equilibrium process	equilibrium constant (25 °C, M^{-1})	$\Delta\bar{G}°$ (kcal)	$\Delta\bar{H}°$ (kcal)	$T\Delta\bar{S}°$ (kcal)
D + CO → D–CO	β_1 = 11 200 ± 2400[a]	−5.5 ± 0.1	−9 ± 5	−4 ± 5
D + 2CO → D–$(CO)_2$	β_2 = 3.1 (±1.3) × 10^7	−10.2 ± 0.2	−18 ± 10	−8 ± 10
2M–CO → D–$(CO)_2$	L_2 = 450 ± 200	−3.6 ± 0.3	−38 ± 10	−34 ± 10
D + 2CO → 2M–CO	K_T = 70 000 ± 40 000	−6.6 ± 0.5	20 ● 4[b]	27 ± 4

[a] Constants were converted from torr units to molarity units by the factor 1.26 × 10^{-6} [mol of CO/(L·atm)] at 25 °C (Wilhelm et al., 1977) and then converted from intrinsic constants to overall constants according to the relationships $\beta_1 = 2\kappa_D$ and $\beta_2 = \kappa_D^2$. [b] This value is estimated from direct calorimetric determinations.

of sites, m_0, is equal to the number of sites per dimer times the partial derivative of Q with respect to the logarithm of the concentration of unligated dimer (Wyman, 1984), the following expression can be solved as a quadratic equation in the square root of [D].

$$m_0 = \frac{2\partial Q}{\partial \ln [D]} = 2(1 + \kappa_D a_x)^2[D] + \frac{\kappa_D a_x}{\sqrt{L_2}}\sqrt{[D]} \quad (6)$$

The calculated value for [D] is then inserted into eq 5 to solve for the fraction of sites bound with ligand.

Equations 5 and 6 were combined with eq 1 to calculate optical density changes as a function of stepwise dilutions of the partial pressure of CO. Binding curve data were taken on three samples, each having a different protein concentration but otherwise identical solution conditions. All three data sets were then combined into a single curve-fitting procedure to resolve the model parameters κ_D and L_2 where only the total concentration of heme sites was changed in eq 5 to fit each set of binding data in Figure 2. A Marquardt nonlinear least-squares fitting program (Bevington, 1969) gave best-fit values for the model parameters as κ_D = 5600 ± 1200 M^{-1} and L_2 = 450 ± 200 M^{-1} at 25 °C. As shown by the theoretical curve in Figure 2 this two-parameter model provides a good general description of this complex CO binding system. The standard error of a point for fitting the optical density change data to the dissociating model, 1.4 × 10^{-3}, is significantly better than the error of 2.5 × 10^{-3} determined for fitting with the nondissociating model shown in Figure 1. In addition the CO-linked dissociation model allows for the asymmetry in the shape of the binding curve data which is a requirement for ligand-linked aggregation processes (Colosimo et al., 1976) but is disallowed by a two-site nondissociating model.

Standard free energy changes were calculated from the fitted equilibrium constants of the dissociating model. These values are given in Table I. The standard-state free energy level diagram in Figure 6 conveniently portrays the relative standard-state free energy levels of all observed macromolecular species involved in the CO-linked dissociating model. From the relative positions of the free energy levels, the general structural and functional features of the macromolecule, as they relate to CO binding, can be predicted. First of all, in the unligated state the lowest free energy form of the macromolecule must be the dimer form. Although not directly observed, the unligated monomer state must lie above the unligated dimer state. This is consistent with two lines of evidence: (1) sedimentation studies show that the reduced dimer form is tightly associated, even in the presence of 6 M

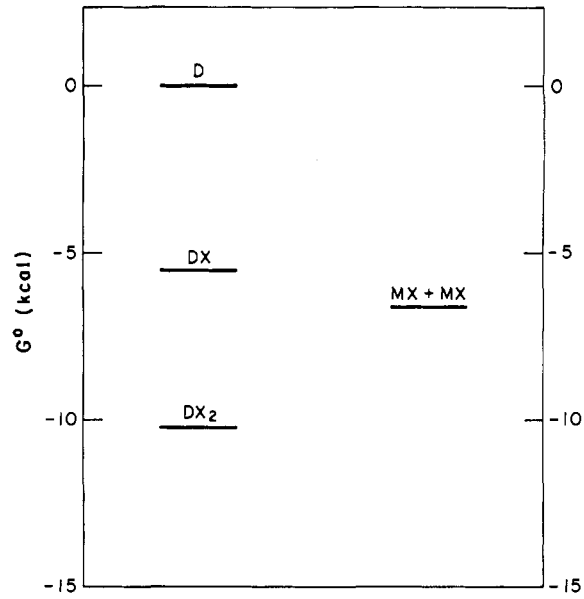

FIGURE 6: Standard-state free energy level diagram for the states of unligated and ligated forms of *C. vinosum* cytochrome *c′*. Standard-state free energy values, $G°$, were calculated from equilibrium constants given in Table I. All free energy levels are given relative to the unligated dimer form which is assigned a free energy of zero. The relative position of the unligated monomer form is not accessible from the present data but must lie above the unligated dimer state.

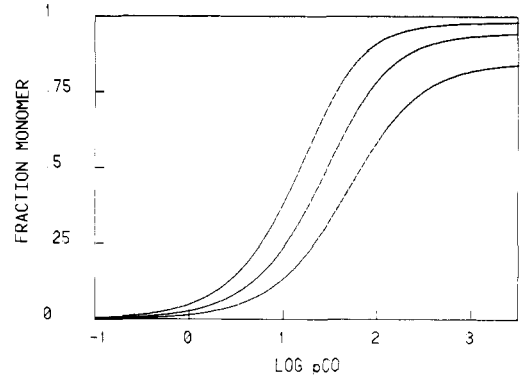

FIGURE 7: Fraction of *C. vinosum* cytochrome *c′* subunits dissociated to the monomer form as a function of the partial pressure of CO. The theoretical curves were generated from the CO-linked association–dissociation model outlined in the text with the equilibrium constants given in Table I. Experimental conditions were 25 °C, pH 7.2 and 100 mM potassium phosphate with protein concentrations (left to right) 20, 70, and 250 μM heme.

Gdn-HCl (Cusanovich, 1971), and (2) the molecular weight was measured by gel filtration (Figure 5) at very dilute protein concentrations (50–0.1 μM heme) and no detectable monomer was observed. Second, two ligated monomers have a slightly higher free energy than fully ligated dimer under standard-state (1 M) conditions. At low concentrations ligated monomer is preferred, which results in dissociation of the ligated dimer form. The general result at low concentrations is that the population of macromolecular species shifts from dimer form to monomer form as the activity of CO increases. Figure 7 shows the population of sites converted to the monomer form as a function of the partial pressure of CO at different protein concentrations. Since the dimer form dissociates when fully ligated, this means the intrinsic CO affinity is greater to the monomer than to the dimer and the binding curve will show positive cooperativity. As seen, the Hill plots in Figure 8 display positive cooperativity. The lowest line represents CO binding to the pure nondissociating dimer form, and there

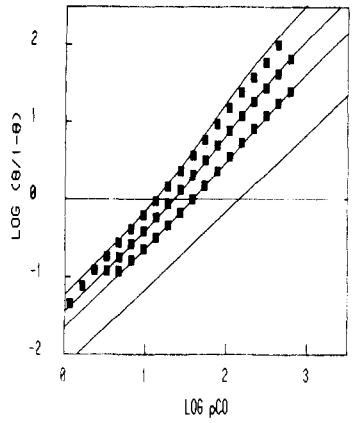

FIGURE 8: Hill plots of CO binding to *C. vinosum* cytochrome *c'* for three concentrations of protein. Experimental conditions were 25 °C, pH 7.2, and 100 mM potassium phosphate buffer. The concentrations of protein were (left to right) 20, 70, and 250 μM heme. The solid lines represent theoretical curves for the CO-linked monomer–dimer equilibrium by using the equilibrium constants given in Table I. The theoretical lower line represents CO binding to pure nondissociated dimer.

presumably would also be an upper line reflecting the unobserved high-affinity binding to the monomer form as well.

Enthalpy and Entropy Contributions to Free Energy Changes. As noted, CO binding to *C. vinosum* cytochrome *c'* is accompanied by an endothermic enthalpy change that is opposite to typical CO binding reactions to heme proteins. A disaggregation process accompanying CO ligation to the dimer is found to explain the observed endothermic effect. The scheme in eq 7 displays the enthalpy changes for all processes

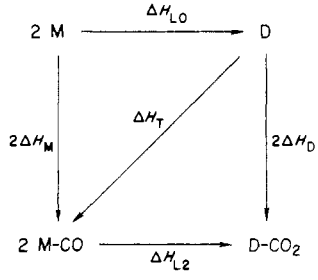

(7)

contributing to the overall enthalpy change for CO binding to *C. vinosum* cytochrome *c'* according to the model of eq 3. Here ΔH_M and ΔH_D are the enthalpy changes for CO binding to the monomer and dimer forms, respectively. The enthalpy change for the monomer–dimer aggregation process in the unligated and fully ligated states are given by ΔH_{L0} and ΔH_{L2}, respectively. The total enthalpy change in going from the unligated dimer state to the ligated monomer state, i.e., along the diagonal, is given by ΔH_T. As noted above the equilibrium between the unligated monomer and dimer lies far to the dimer side under the range of protein concentrations studied in the present analysis. Thus, only the reactions described by the lower right-hand triangle in eq 7 are accessible from the present data, and reactions giving ΔH_M and ΔH_{L0} are inaccessible. The accessible enthalpy changes were determined by combination of two independent methods, calorimetry and a temperature dependence study of the binding curve.

Temperature-dependent changes in shape and location of the CO binding curve are a function of the enthalpy changes described by eq 7. To estimate these enthalpy values, binding curves were measured at four different temperatures, and each temperature was studied at three different protein concentrations. All 12 data sets were then fitted simultaneously to eq 1 by using temperature-dependent forms of the equilibrium constants in eq 5 and 6. In general an equilibrium constant that varies linearly with temperature is given as a function of temperature as

$$K = K^0 e^{(-\Delta H/R)[(1/T)-(1/T_0)]} \quad (8)$$

where the observed equilibrium constant at temperature T is K and the equilibrium constant at a reference temperature T_0 is K^0. The enthalpy change for the equilibrium process is ΔH, and R is the gas constant. The reference temperature was taken as 298 K, and the equilibrium constants at the reference temperature, $\kappa_D°$ and $L_2°$, are given above. The fitting procedure resolved values of $\Delta H_D = -9 \pm 5$ kcal/mol of CO(aq) and $\Delta H_{L2} = -38 \pm 10$ kcal/mol of dimer from the data. Figure 3 summarizes the temperature and protein concentration dependence of the CO binding reaction to *C. vinosum* cytochrome *c'* in terms of the median partial pressure values, p_m, for each binding curve measurement. The p_m value for a given binding curve is the point on the binding curve where the areas above and below the curve are equal. The values shown in Figure 3 are experimental values determined by integration. The theoretical curves in Figure 3 were generated by using the CO-linked dissociation model with the parameters in Table I. The detailed expression for calculation of p_m values for the CO-linked dissociation model is given in the Appendix. The satisfactory agreement with the median data as a function of both temperature and protein concentration, along with the chromatographic results, indicates the overall consistency of the present model.

Calorimetry experiments of CO binding to the essentially pure dimeric state to produce essentially ligated monomer provide the best determination of ΔH_T shown as the diagonal process in eq 7. The data shown in Figure 4 represent heats for injecting the unligated reduced cytochrome *c'* into a buffer solution containing an excess of CO. The observed heat changes are, to a first approximation, equal to the overall heat of CO ligation to the macromolecule, since the protein becomes about 98% saturated with CO under the experimental conditions. The extent of ligated monomer form compared to dimer also depends on the total heme concentration as illustrated in Figure 7, and in the range of 20–100 μM heme the fully ligated material is essentially in the monomeric form. Thus, the observed calorimetric measurements are describing the process of going from unligated dimer to ligated monomer. The value for ΔH_T in solution was determined as 10 ± 2 kcal/mol of heme, or 20 ± 4 kcal/mol of dimer.

The enthalpy change for CO binding to the dimer form, -9 ± 5 kcal/mol of CO(aq) is normal for CO binding to heme proteins and is comparable to the value of -11 ± 1 kcal/mol of CO(aq) determined for CO ligation to dimeric *R. molischianum* cytochrome *c'* (Doyle & Gill, 1985). However, the overall endothermic effect we observe for CO ligation is clearly due to the large endothermic heat of dissociation of ligated dimer into monomers. This dissociation is also accompanied by a large increase in entropy. The observed large positive entropy change for the CO-ligated dimer dissociation is opposite in sign to that expected if exposure of hydrophobic groups were the primary factor in this term. This suggests that significant structural change occurs in the subunits upon dissociation of the ligated dimer to monomer, presumably leading to a more disordered state. Unfortunately there is as yet no crystallographic information on a CO-ligated species to confirm this suggestion. However, consistent with this suggestion is work done on *R. rubrum* cytochrome *c'* which demonstrated that dissociation of the oxidized form of the dimer into monomers is accompanied by significant loss in secondary structure (Akutsu et al., 1983; Imai et al., 1969).

The molecular origin of these unusual enthalpy and entropy terms is suggested from the features of the crystal structure of the closely related molecule *R. molischianum* cytochrome *c′*. The *R. molischianum* structure shows stabilization of the dimer form by interfacial hydrophobic contacts and at least two salt bridges (Weber et al., 1981). Comparison of the amino acid sequences of *C. vinosum* cytochrome *c′* and *R. molischianum* cytochrome *c′* (Ambler et al., 1981) shows many alterations in primary sequence, particularly in the intersubunit contact region. One key difference between these molecules is that the residues responsible for the salt bridges in the *R. molischianum* structure are altered in the *C. vinosum* primary sequence. Thus, the *Chromatium* structure is unable to form these stabilizing salt bridges.

As mentioned above the unligated monomer to dimer equilibrium lies far to the right in the range of protein concentrations studied. The gel chromatography experiments were done on protein concentrations as low as 0.1 μM heme with no indication of dissociation of the unligated dimer. This implies a dissociation constant for the reaction lower than 10^{-7} M, representing a highly stable unligated dimeric state. In previous studies the dimer form did not dissociate, even in the presence of 6 M guanidine (Cusanovich, 1971). One striking feature of this system is the large shift in the monomer–dimer dissociation constant from lower than 10^{-7} M in the unligated form to about 2×10^{-3} M in the CO-bound form. Such a large shift reflects the sensitivity of the interfacial contact region to the state of CO ligation.

Previous kinetic and equilibrium CO binding studies on *C. vinosum* cytochrome *c′* have shown that this material exhibited multistep kinetic processes and an unusual stoichiometry (Cusanovich & Gibson, 1973). The results suggested a stoichiometry of binding two CO molecules for each polypeptide chain containing a single heme group. This suggestion was based in part on the assumption that the dimeric molecule remained dimeric upon CO ligation. Reevaluation of the earlier binding data in terms of the CO-linked dissociation process shows that a stoichiometry of 1 mol of CO per polypeptide chain accounts for their observed results. [Further evidence in support of a 1:1 stoichiometry comes from calorimetric CO binding studies on *R. molischianum* cytochrome *c′* which yield a stoichiometry equal to one molecule of CO per heme (Doyle & Gill, 1985)]. The multistep kinetic process invoked to explain the kinetics of CO binding to *C. vinosum* cytochrome *c′* can now be argued to have its origin in the ligand-dependent dissociation reaction as well.

Since analysis of ligand binding data becomes more complicated as the number of binding sites increases, the simplest system to study ligand-linked site–site interactions is that of a two-site macromolecule. In this regard the cytochromes *c′* are especially attractive for detailed investigations of the energetics of ligand-linked macromolecular processes.

Appendix

The median partial pressure, p_m, for the monomer–dimer model in eq 3 may be evaluated by considering the condition of equal areas above and below the θ vs. ln p_{CO} binding curve (Wyman, 1964). The area under the curve is given by

$$A_u = \int_{x=0}^{x} \theta \, d \ln a_x \tag{A1}$$

and the area above the curve by

$$A_a = \int_{x}^{x=\infty} (1 - \theta) \, d \ln a_x \tag{A2}$$

where θ is the fraction of sites bound with ligand at specified partial pressure or activity a_x. These equations may be evaluated by first noting that the derivative of the partition function in the two variables ln a_x and ln [D] is

$$dQ = \frac{\partial Q}{\partial \ln a_x} d \ln a_x + \frac{\partial Q}{\partial \ln [D]} d \ln [D] \tag{A3}$$

Substitution of the first parts of eq 5 and 6 yields

$$dQ = m_0 \theta d \ln a_x + \frac{m_0}{2} d \ln [D] \tag{A4}$$

Introduction of eq A4 into eq A1 and A2, and then equating them, leads directly for the case under consideration to the expression

$$\ln p_m = \frac{Q_0 - Q_\infty}{m_0} + \ln \frac{f}{\sqrt{[D]_0}} \tag{A5}$$

where Q_0 and Q_∞ are the partition functions at zero and infinite ligand activities, m_0 is the heme site concentration, and $[D]_0$ is the unligated dimer concentration at zero ligand activity. The term f is defined as a finite value, $([D]_\infty)^{1/2} a_{x\infty}$, which is the product of the square root of the unligated dimer concentration and the ligand activity as this activity becomes infinite. The value of f is determined by the quadratic equation expressing the heme mass balance at infinite activity ($m_0 = 2\kappa_D^2 f^2 + \kappa_D f / L_2^{1/2}$). The values of Q_0 and Q_∞ are then determined for the system by using eq 4 as

$$\frac{Q_0}{m_0} = \frac{[D]_0}{m_0} = \frac{1}{2} \tag{A6}$$

$$\frac{Q_\infty}{m_0} = \frac{\frac{1}{4\kappa_D}\left(\frac{-\kappa_D}{\sqrt{L_2}} + \sqrt{\frac{\kappa_D^2}{L_2} + 8\kappa_D^2 m_0}\right) + \frac{1}{\sqrt{L_2}}}{\frac{1}{2\kappa_D}\left(\frac{-\kappa_D}{\sqrt{L_2}} + \sqrt{\frac{\kappa_D^2}{L_2} + 8\kappa_D^2 m_0}\right) + \frac{1}{\sqrt{L_2}}} \tag{A7}$$

$$\frac{f}{\sqrt{[D]_0}} = \frac{-\frac{\kappa_D}{\sqrt{L_2}} + \sqrt{\frac{\kappa_D^2}{L_2} + 8\kappa_D^2 m_0}}{4\kappa_D^2} \frac{\sqrt{2}}{\sqrt{m_0}} \tag{A8}$$

The temperature dependence of these expressions is given in terms of the appropriate van't Hoff relations for each equilibrium constant.

Registry No. CO, 630-08-0; cytochrome *c′*, 9035-41-0.

References

Ackers, G. K., & Halvorson, H. R. (1974) *Proc. Natl. Acad. Sci. U.S.A. 71*, 4312–4316.

Adair, G. S. (1925) *J. Biol. Chem. 63*, 529.

Akutsu, H., Kyogoku, Y., & Horio, T. (1983) *Biochemistry 22*, 2055–2061.

Ambler, R. P., Bartsch, R. G., Daniel, M., Kamen, M. D., McClellan, L., Meyer, T. E., & Van Beeumen, J. (1981) *Proc. Natl. Acad. Sci. U.S.A. 78*, 6854–6857.

Antonini, E., & Brunori, M. (1971) in *Hemoglobin and Myoglobin in Their Reactions with Ligands* (Neuberger, A., & Tatum, E. L., Eds.) North-Holland, Amsterdam.

Bartsch, R. G. (1971) *Methods Enzymol. 23*, 344–363.

Bartsch, R. G. (1978) in *The Photosynthetic Bacteria* (Clayton, R. K., & Sistrom, W. R., Eds.) pp 249–280, Plenum, New York.

Bevington, P. R. (1969) in *Data Reduction and Error Analysis for the Physical Sciences*, McGraw-Hill, New York.
Cusanovich, M. A. (1971) *Biochim. Biophys. Acta 236*, 238–241.
Cusanovich, M. A., & Gibson, Q. H. (1973) *J. Biol. Chem. 248*, 822–834.
Colosimo, A., Brunori, M., & Wyman, J. (1976) *J. Mol. Biol. 100*, 47–57.
Dolman, D., & Gill, S. J. (1978) *Anal. Biochem. 87*, 127–134.
Doyle, M. L., & Gill, S. J. (1985) *J. Biol. Chem. 260*, 9534–9536.
Doyle, M. L., Weber, P. C., & Gill, S. J. (1985) *Biochemistry 24*, 1987–1991.
Hayashi, A., Suzuki, T., & Shin, M. (1973) *Biochim. Biophys. Acta 310*, 309–316.
Hill, A. V. (1910) *J. Physiol. (London) 40*, iv–vii.
Imai, Y., Imai, K., Ikeda, K., Hamaguchi, K., & Horio, T. (1969) *J. Biochem. (Tokyo) 65*, 629–637.
Kassner, R. J., Rubinow, S. C., & Cusanovich, M. A. (1983) *Biochim. Biophys. Acta 743*, 195–199.
Kennel, S. J., Meyer, T. E., Kamen, M. D., & Bartsch, R. G. (1972) *Proc. Natl. Acad. Sci. U.S.A. 69*, 3432–3435.
McKinnon, I. R., Fall, L., Parody-Morreale, A., & Gill, S. J. (1984) *Anal. Biochem. 139*, 134–139.
Meyer, T. E., & Kamen, M. D. (1982) *Adv. Protein Chem. 35*, 105–212.
Rubinow, S. C., & Kassner, R. J. (1984) *Biochemistry 23*, 2590–2595.
Taniguchi, S., & Kamen, M. D. (1963) *Biochim. Biophys. Acta 74*, 438–455.
Weber, P. C., Howard, A., Huu Xuong, N., & Salemme, F. R. (1981) *J. Mol. Biol. 153*, 399–424.
Wilhelm, E., Battino, R., & Wilcock, R. J. (1977) *Chem. Rev. 77*, 219–262.
Wyman, J. (1965) *J. Mol. Biol. 11*, 631.
Wyman, J. (1984) *Q. Rev. Biophys. 17*, 453–488.

Oxidation–Reduction Properties of Glycolate Oxidase†

Charles Pace and Marian Stankovich*
Department of Chemistry, University of Minnesota, Minneapolis, Minnesota 55455
Received August 13, 1985; Revised Manuscript Received December 31, 1985

ABSTRACT: This is the first report of the redox potentials of glycolate oxidase. The pH dependence of the redox behavior as well as the effects of activators and inhibitors was studied. At pH 7.1 in 10 mM imidazole–chloride, $E_1^{\circ\prime}$ ($EF1_{ox}/EF1^{-}\cdot$) is -0.033 ± 0.010 V and $E_2^{\circ\prime}$ ($EF1^{-}\cdot/EF1_{red}H^{-}$) is -0.017 ± 0.017 V vs. the standard hydrogen electrode at 10 °C. A maximum of 29% flavin mononucleotide (FMN) anion radical is stabilized at half-reduction at pH 7.1 and 10 °C. Both redox couples of glycolate oxidase are pH-dependent from pH 7 to pH 9, and the FMN anion radical is stabilized in this range. The redox potentials of glycolate oxidase are shifted markedly positive of those of unbound FMN, consistent with the enzyme's function. The midpoint potential of glycolate oxidase is more positive than that of the glyoxalate/glycolate couple, and two-electron reduction of glycolate oxidase is thermodynamically favorable. The redox behavior of glycolate oxidase markedly contrasts that of other flavoprotein oxidases. For most flavoprotein oxidases, $E_1^{\circ\prime}$ is independent of pH from pH 7 to pH 9 and is much more positive than $E_2^{\circ\prime}$, which is pH-dependent. We present a mechanism that suggests a structural basis for the positive shifts and pH dependence of both $E_1^{\circ\prime}$ and $E_2^{\circ\prime}$ of glycolate oxidase.

Glycolate oxidase (glycolate:oxygen oxidoreductase, EC 1.1.3.1) catalyzes oxidation of α-hydroxy acids by molecular oxygen to produce α-keto acids and hydrogen peroxide. Previous studies of the isolated enzyme from pig liver have explored its physicochemical and steady-state kinetic properties (Dickinson & Massey, 1963; Schuman & Massey, 1971a,b). Particular attention was paid to the spectral and kinetic effects of mono- and dianions, e.g., chloride or oxalate ions. These anions are inhibitors except for phosphate and arsenate, which are activators (Schuman & Massey, 1971b).

A consistent picture of the redox behavior and structure of free and inhibitor-bound flavoprotein oxidases has emerged from electrochemical studies conducted in this laboratory (Stankovich & Fox, 1983, 1984; Van den Berghe-Snorek & Stankovich, 1985). Briefly, E_m[1] for flavin in flavoprotein oxidases is shifted positive relative to E_m for uncomplexed flavin. The positive shift is more pronounced for $E_1^{\circ\prime}$ than for $E_2^{\circ\prime}$. In addition, $E_1^{\circ\prime}$ for L-amino acid oxidase or D-amino acid oxidase is pH-independent from pH 7 to pH 9 but $E_2^{\circ\prime}$ is pH-dependent.

We wondered whether or not glycolate oxidase fit this pattern and whether or not the redox properties of glycolate oxidase were changed by binding of activators and inhibitors. Previously, redox titration of native glycolate oxidase had not

† This work was supported by a grant from the National Institutes of Health (GM 29344).

[1] Abbreviations: FMN, flavin mononucleotide; $EF1_{ox}$, glycolate oxidase with oxidized FMN cofactor; $EF1^{-}\cdot$, glycolate oxidase with the FMN cofactor in the anion radical form; $EF1_{red}H^{-}$, glycolate oxidase with reduced FMN cofactor; E_m, midpoint potential; $E_1^{\circ\prime}$, formal potential for the redox couple oxidized flavin/flavin radical; $E_2^{\circ\prime}$, formal potential for the redox couple flavin radical/reduced flavin; AMPD, 2-amino-2-methyl-1,3-propanediol; CD, circular dichroism; 8CR, 8-chlororiboflavin; EDTA, ethylenediaminetetraacetate; IDS, indigo disulfonate; $MV^{+}\cdot$, methyl viologen radical; Pyo, pyocyanine; PSF, phenosafranine; SHE, standard hydrogen electrode; TEA, triethanolamine; Tris, tris(hydroxymethyl)aminomethane.

0006-2960/86/0425-2516$01.50/0